# Rational design of multifunctional polymeric nanoparticles based on poly(L-histidine) and d-#-Vitamin E Succinate for reversing tumor multidrug resistance

Zhen Li, Qixian Chen, Yan Qi, Zhihao Liu, Tangna Hao, Xiaoxin Sun, Mingxi Qiao, Xiaodong Ma, Ting Xu, Xiuli Zhao, Chunrong Yang, and Dawei Chen

*Biomacromolecules*, **Just Accepted Manuscript** • DOI: 10.1021/acs.biomac.8b00213 • Publication Date (Web): 04 Apr 2018

# Rational design of multifunctional polymeric nanoparticles based on poly(L-histidine) and d-α-Vitamin E Succinate for reversing tumor multidrug resistance

Zhen Li[a,b,*], Qixian Chen[c], Yan Qi[a], Zhihao Liu[a], Tangna Hao[d], Xiaoxin Sun[e], Mingxi Qiao[b], Xiaodong Ma[a], Ting Xu[c], Xiuli Zhao[b], Chunrong Yang[f,*], Dawei Chen[b,g,*]

[a] School of Pharmacy, Dalian Medical University, Dalian, 116044, PR China

[b] Department of Pharmaceutics, School of Pharmacy, Shenyang Pharmaceutical University, Shenyang, 110016, PR China

[c] School of Life Science and Biotechnology, Dalian University of Technology, 116024, PR China

[d] Department of Pharmacy, The Second Affiliated Hospital of Dalian Medical University, Dalian, 116011, PR China

[e] Institute (College) of Integrative Medicine, Dalian Medical University, Dalian 116044, PR China

[f] School of pharmacy, Jiamusi University, Jiamusi 154007, PR China

[g] School of Pharmacy, Medical College of Soochow University, Suzhou 215123, PR China

Correspnding author: Zhen Li*

Email: lizhenpharm@126.com

Corresponding author: Chunrong Yang*

Email: jmsyangchunrong@163.com

Corresponding author: Dawei Chen*

E-mail: chendawei@syphu.edu.cn

**ABSTRACT**

A multifunctional nanoparticulate system composed of methoxy poly(ethylene glycol)-poly(L-histidine)-d-α-Vitamin E succinate (MPEG-PLH-VES) copolymers for encapsulation of doxorubicin (DOX) was elaborated with the aim of circumventing the multidrug resistance (MDR) in breast cancer treatment. The MPEG-PLH-VES nanoparticles (NPs) were subsequently functionalized with biotin motif for targeted drug delivery. The MPEG-PLH-VES copolymer exert no obvious effect on the P-gp expression level of MCF-7/ADR but exhibited a significant influence on the loss of mitochondrial membrane potential, the reduction of intracellular ATP level and the inhibition of P-gp ATPase activity of MCF-7/ADR cells. The constructed MPEG-PLH-VES NPs exhibited an acidic pH-induced increase on particle size in aqueous solution. The DOX-encapsulated MPEG-PLH-VES/biotin-PEG-VES (MPEG-PLH-VES/B) NPs were characterized to possess high drug encapsulation efficiency of approximate 90%, an average particle size of approximate 130 nm and a pH-responsive drug release profile in acidic milieu. Confocal laser scanning microscopy (CLSM) investigations revealed that the DOX-loaded NPs resulted in an effective delivery of DOX into MCF-/ADR cells and a notable carrier-facilitated escape from endo-lysosomal entrapment. Pertaining to the *in vitro* cytotoxicity evaluation, the DOX-loaded MPEG-PLH-VES/B NPs resulted in more pronounced cytotoxicity to MCF-/ADR cells comparing with DOX-loaded MPEG-PLH-VES NPs and free DOX solution. *In vivo* imaging study in MCF-7/ADR tumor-engrafted mice exhibited that the MPEG-PLH-VES/B NPs accumulated at the tumor site more

effectively than MPEG-PLH-VES NPs due to the biotin-mediated active targeting effect. In accordance with the *in vitro* results, DOX-loaded MPEG-PLH-VES/B NPs showed the strongest inhibitory effect against the MCF-7/ADR xenografted tumors with negligible systemic toxicity, as evidenced by the histological analysis and change of body weight. The multifunctional MPEG-PLH-VES/B nanoparticulate system has been demonstrated to provide a promising strategy for efficient delivery of DOX into MCF-7/ADR cancerous cells and reversing MDR.

KEYWORDS: MPEG-PLH-VES copolymer; self-assembled nanoparticles; doxorubicin; multidrug resistance; P-gp function; targeted delivery; antitumor activity

## 1. INTRODUCTION

The failure of chemotherapy is acknowledged to associate with the occurrence of multidrug resistance (MDR), where the cancerous cells simultaneously display resistance to a wide range of chemotherapeutics despite single chemotherapeutic drug was administered. There are several molecular mechanisms underlying the acquired MDR propensity: (1) increased drug efflux; (2) reduced drug influx; (3) improved DNA repair activity; (4) changes in drug metabolism; (5) reluctant apoptosis in accompanied with possession of anti-apoptotic defensing mechanisms; (6) genomic amplification or mutation of relevant proteins and (7) sequestration of drugs within cytoplasmic vesicles[1-3]. Indeed, the acquired MDR of the cancer cells involves a series of cellular processes. Particularly, multiple mechanisms may simultaneously conduce to the cellular drug resistance. Therefore, it is an onerous task to design an adequate drug delivery system to achieve maximal reversal of MDR.

P-glycoprotein (P-gp), characterized with a member of ATP-binding cassette family, has been documented to be one of the main drug efflux transporters to induce efflux-mediated MDR[4]. A number of chemotherapeutic drugs (e.g. doxorubicin, etoposide, vinblastine and paclitaxel) are determined to be P-gp-substrates. Hence, P-gp is capable of pumping substrates out of tumor cells using the energy of ATP-hydrolysis, and thus resulting in reduced intracellular drug accumulation[5]. The anti-cancer drug-loaded nanocarriers internalized by endocytosis offer a promising therapeutic approach to evade and bypass the P-gp mediated cellular efflux[6-8]. To this respect, a string of natural and synthetic polymers has been developed for

manufacture of nanocarriers with the intention of improving cellular accumulation of chemotherapeutic drugs. Unfortunately, most of the intracellular drug molecules could still be pumped out by efflux proteins because the ordinary polymeric nanomaterials lack of adequate facilities on inhibiting efflux pump[9, 10]. Hence, it requests the design of functional polymeric nanomaterials in affording P-gp inhibition functionality so as to further improve the potency of the chemotherapeutic activity. Some nonionic surfactants, including Tween 80, Poloxamer, Cremophor EL and D-α-Tocopheryl polyethylene glycol succinate 1000 (TPGS), have demonstrated the ability in inhibiting the P-gp activity[11]. Particularly, TPGS is one of the most promising surfactants for the reversal of MDR. Vitamin E succinate (VES) exists as the hydrophobic moiety of TPGS and acts a vital part in the sensitization of MDR cells by inhibiting the substrate-induced ATPase activity[12]. TPGS can also be utilized as emulsifier, solubilizer, absorption enhancer, and a component material of nanocarriers[13]. In addition, TPGS has been proved to possess micellar properties, as evidenced by formation of stable micelles in aqueous solution[14].

Despite important characters of TPGS micelles for the drug delivery applications, considerable drawbacks are imperative to be resolved for their translation into wide *in vivo* availabilities[12, 15]. One major disadvantage is the relatively small molecular weight of PEG chain (Mw: 1000 Da) of TPGS, which led to poor capacity in diminishing the immune-reaction (e.g. adsorption of micelles onto the phagocytes) and poor persistence in the bloodstream post systemic dosage. To this regard, some attempts have been made to overcome the aforementioned drawback of TPGS. For

instance, Mi et al synthesized the hybrid of TPGS 2000 and TPGS3350-Folate conjugates, followed by self-assembly for construction of micelles to pursue targeted docetaxel delivery[16]. TPGS 2000 was characterized to possess a lower CMC value (0.0219 mg/ml) relative to that of the original TPGS (0.2 mg/ml). Moreover, the TPGS 2000 conjugate itself exerted anti-cancer activity by mean of substituting ubiquinone from binding to complex II in the mitochondrial respiratory chain, which consequently promoted a synergistic interaction with the formulated drug. Besides, some other nanomedicines based on PEG-derivatized VES conjugates have also been developed to enhance the anti-metastatic performance of the loaded chemotherapeutic drugs, overcome MDR in chemotherapy, and enhance the antitumor therapeutic efficacy[17-20]. Therefore, such analogs of TPGS (retaining the structure of VES moiety) hold promise as an improved nanoparticulate formulation and deserve further investigations for cancer treatments.

Compared to molecular drug, the polymeric nanocarriers enable improved the accumulation and delivery of loaded chemotherapeutics agents to the tumors via the enhanced permeability and retention (EPR) effect[21, 22]. Unfortunately, in many cases the drug release from polymer-based nanocarriers is characterized to exhibit a retarded process, thereby becoming difficult to reach an effective therapeutic level at the target sites. This is the particular obstacle to attain adequate anti-tumor efficacy to the tumors with abundance composition of drug-resistant cancer cells[23, 24]. This fact encouraged the pharmaceutic researchers to develop the functional nanoparticulate systems with triggering drug release profiles responsive to external or internal stimuli

(e.g. temperature, light, pH, reductive glutathione (GSH), enzymes and ultrasound)[25-30]. Noteworthy was the modality of pH-sensitive polymeric nanocarriers, which has experienced progressive development for the medical and biological applications. For instance, the extracellular pH in most tumors is estimated to be mild acidic (pH 6.5-7.2) in contrast to the physiological milieu (pH 7.4). Moreover, subcellular compartments of endosomes and lysosomes are characterized to possess more acidic conditions (pH 4.0-6.0)[31]. In addition, MDR cancer cells have the propensity of creating more acidic organelles (such as recycling endosome, lysosome and trans-Golgi network) comparing with the drug-vulnerable cancer cells[32]. Based on the aforementioned physiological characters, poly(L-histidine) (PLH) was often harnessed as an excellent pH-sensitive candidate due to its distinct pH-responsive characters. It is a peptide containing imidazole groups with a pKa value of 6.0-7.0. The protonation of PLH would occur when the environmental pH is below the pKa of PLH[33]. A string of pH-responsive formulations based on PLH have been design with the aim of intelligently controlling the drug release at different pH environments[33-35]. The designed nanoparticulate systems were anticipated to maintain the stability in blood circulation environment (pH 7.4) and suffer structural destabilization in relatively acidic pH environment (such endosomes and lysosomes) due to the promoted protonation of PLH. Furthermore, the protonated PLH can interact with anionic phospholipids (membrane components of the endo-lysosomal compartments) and result in appreciable endo-lysosomal membranes disruption[36]. The postulated activity is particular vital in facilitating the effective delivery of drugs into the

cytoplasm to pursue improved potency to the affected tumor cells.

Aiming to facilitate the tumor-specific drug transportation, the surface of the nanocarriers can be functionalized with various tumor-targeting moieties, including peptides, aptamers, saccharides, folate and biotin[37-41]. Of note, biotin is a water-soluble B-vitamin which acts a critical part in nourishing the healthy hair, nails and skin[42]. Cancer cells requests a markedly larger amount of vitamins (such as folate, biotin and vitamin B12) to sustain its proliferation, thereby inducing overexpress of wide range of vitamin receptors on the cell surfaces[41]. Hence, the specific interactions between vitamins and their receptors could be harnessed for pursuit of targeted drug delivery. In respect to the simply chemical structure, low molecular weight and good reactivity, biotin has been extensively explored for utilities as the targeting moiety for tumor-targeted therapeutics. The uptake of biotin could be facilitated by streptavidin-avidin receptors and/or sodium-dependent multivitamin transporter on the surface of cancer cells[43]. In pertinent to nanomedicines, biodegradable polymeric nanocarriers with functionalization of biotin have been determined to mediate higher level of the cellular uptake activities in many cancer cell lines (including MCF-7 and MCF-7/ADR cells utilized here) than non-functionalized nanocarriers [44-48].

Motivated by the abovementioned rationales, we firstly synthesized a novel amphiphilic polymer–methoxy poly(ethyleneglycol)-poly(L-histidine)-d-α-Vitamin E Succinate (MPEG-PLH-VES), which was anticipated to encompass the aforementioned advantages of both VES and PLH. The MPEG-PLH-VES copolymers were mixed with the home-made biotin-PEG-VES conjugates to form a novel

nanoparticulate system for targeted and intracellular transportation of DOX (an effective anticancer agent). The physiological characteristics (e.g. drug encapsulation efficiency, particle size, zeta potential and *in vitro* drug release behavior) of the DOX-loaded NPs were performed. The antitumor efficacy and MDR reversal mechanisms of the DOX-loaded NPs were systematically evaluated both *in vitro* and *in vivo*. These investigations validated the rationale of the proposed multifunctional polymeric NPs, capable of efficiently encapsulating the chemotherapeutic drug of DOX, promoting the activity of MCF-7/ADR cell internalization and tumor accumulation, specifically accelerating intracellular release of the encapsulated DOX responsive to the intracellular acidic subcellular compartment, retrieving DOX from endo-lysosomal entrapment, exerting the MDR reversal effect and minimizing systemic toxicity of DOX.

## 2. MATERIALS AND METHODS

### *2.1. Synthesis of MPEG-PLH-VES and biotin-PEG-VES*

#### *2.1.1. Synthesis of the protected MPEG-PLH*

Anhydrous THF (15 mL) containing $N^{\alpha}$-CBZ-$N^{im}$-DNP-L-histidine (3 g, 6.60 mmol) was drop-wise supplemented with 5 equivalent thionyl chloride. Subsequently, the above reaction solution was agitated for 5 h at 25 °C under protection of nitrogen. The mixture was precipitated in chilled ether, followed by sequential filtration and vacuum-drying. Subsequently, the yielded $N^{im}$-DNP-L-histidine NCA·HCl (2 g, 5.77 mmol) was solubilized in anhydrous DMF (40 mL) as the monomer for ring-opening polymerization with the macro-initiator of methoxypolyethylene glycol amine 2000

(MPEG2000-$NH_2$). The polymerization reaction was performed at 25 °C for 72 h. The yielded MPEG-poly($N^{im}$-DNP-L-histidine) (protected MPEG-PLH) was collected by sequential precipitation in chilled ether and vacuum-drying (yield ca. 64%).

*2.1.2. Synthesis of MPEG-PLH-VES*

VES, NHS and EDC·HCl were solubilized in DMF (10 mL) according to a molar ratio of 1: 1.2: 1.2. The mixture was allowed to stir at room temperature for 4 h, aiming to pre-activate the carboxyl group of VES. Subsequently, the aforementioned MPEG-PLH (1 g, 0.18 mmol) was transferred to the above reaction solution, followed by stirring at 25 °C for 48 h. Afterwards, the resulting solution was transferred for precipitation in chilled ether to obtain the protected MPEG-PLH-VES, followed by vacuum-drying.

The protected MPEG-PLH-VES (1 g, 0.16 mmol) and a precalculated amount of 2-mercaptoethanol were solubilized in DMSO, followed by agitating for 24 h. Subsequently, the above solution was dialyzed against water for 72 h. The end product (MPEG-PLH-VES) was harvested by lyophilization (yield ca. 52%).

*2.1.3. Synthesis of biotin-PEG-VES*

The synthesis procedure of biotin-PEG-VES was detailed in the supporting information.

*2.2. Characterization of the synthesized polymers*

The relevant details were introduced in the supporting information.

*2.3. Acid–base titration of MPEG-PLH-VES*

The MPEG-PLH-VES nanoparticulate solution (1 mg/mL) was initially adjusted

to pH 11 with 1 M NaOH. Furthermore, the diluted solution was titrated with 0.01 M HCl solution by following stepwise manner to construct the titration curve.

*2.4. Preparation and characterization of the polymeric NPs*

The DOX-encapsulated MPEG-PLH-VES NPs and MPEG-PLH-VES/B NPs were prepared as previously described[34]. The corresponding blank NPs were also provided in a similar procedure. The experimental procedures of the NPs preparation, particle size and zeta potential measurement, TEM observation and drug encapsulation efficiency determination were described in the supporting information.

*2.5. In vitro drug release*

The release profiles of DOX from nanoparticles were studied utilizing dialysis method. In brief, 2 mL DOX-loaded NPs solution was dialyzed against 25 mL of release media (pH 7.4 or 5.0) at 37 °C. Periodically, 3 mL aliquots were taken and replaced by 3 mL blank medium. Finally, the released drug amount was quantified with UV-vis spectrometer at 481 nm.

*2.6. Detection of P-gp expression level*

MCF-7/ADR cells were treated with TPGS or MEPG-PLH-VES nanoparticulate solution (final concentration at 50 μM) for 4 h. Subsequently, the cells were trypsinized and fixed with 4% paraformaldehyde. Subsequently, the cells were incubated with rabbit anti-human P-gp antibody (1:25) for 30 min at 4 °C, and centrifugated to remove the unbound antibody. After that the cells were treated with FITC-labeled goat anti-rabbit antibody (1:50) for 30 min. eventually, the cells were rinsed and resuspended in PBS for quantitative fluorescence analysis using a flow

cytometer.

*2.7. Assay of mitochondrial membrane potential*

The MCF-7/ADR cells were incubated with TPGS or MEPG-PLH-VES nanoparticulate solution (final concentration at 50 μM) for 2 h. The mitochondrial membrane potential was determined as previously described[19].

*2.8. Intracellular ATP level assay*

The MCF-7/ADR cells were incubated with TPGS or MEPG-PLH-VES nanoparticulate solution (final concentration at 50 μM) for 2 h. After that, the ATP level was measured as previously described[19].

*2.9. Determination of P-gp ATPase activity*

The effect of MPEG-PLH-VES on P-gp ATPase activity was investigated based on P-gp-Glo assay system (Promega, USA). In brief, varied concentrations of the sample compounds containing verapamil (50 mM) and MPEG-PLH-VES copolymer (final concentration at 0, 10, 50 and 100 μM, respectively) or $Na_3VO_4$ alone were incubated with recombinant P-gp membranes for 5 min at 37 °C. Afterward, the reaction was stimulated by the MgATP for 40 min. Furthermore, the samples were mixed with ATP detection reagent to initiate an ATP-dependent luminescence reaction at room temperature. The luminescence signals were determined by multifunctional microplate reader (Tecan, Austria). The changes of relative light unit (ΔRLU) were acquired by calculating the difference between the $Na_3VO_4$-treated samples and the mixture of polymer and verapamil-treated samples. In addition, the ΔRLU values were plotted as a function of the reciprocal of verapamil concentrations (25, 40, 50

and 100 mM) to acquire the linear regression for each concentration of MPEG-PLH-VES (10 or 100 mM).

*2.10. In vitro cytotoxicity*

The MCF-7 or MCF-7/ADR cells were incubated with free DOX, blank NPs and DOX-encapsulated NPs for 48 h. Afterwards, MTT was added, followed by 4 h incubation. The generated crystals of purple formazan were solubilized in DMSO, followed by determination of the absorbance (at 570 nm) with a microplate reader. The cytotoxicity of blank polymeric NPs on L02 cells (human normal liver cells) was also evaluated with a similar procedure.

*2.11. Cellular uptake and intracellular localization*

MCF-7/ADR cells were treated with DOX-loaded NPs (10 μg/mL DOX-equivalent) for 1 and 4 h. Furthermore, the cells were rinsed and stained with 100 nM Lysotracker Green (5 min) and 10 μg/mL Hoechst 33342 (10 min), aiming to observe lysosomes and nuclei, respectively. Subsequently, the cells were subjected to fixation with 4% paraformaldehyde, followed by being captured utilizing a CLSM (LSM 710, Carl Zeiss). The cellular uptake activities of various DOX formulations were further quantitatively analyzed using flow cytometry as previous described[34].

*2.12. In vivo imaging*

Non-invasive *in vivo* imaging systems were employed to gain insight on the real-time biodistribution activities of DiR-labeled NPs in the female BALB/c nude mice (18-20 g) engrafted MCF-7/ADR tumors. Briefly, each of $1 \times 10^7$ cancerous cells was inoculated into the abdomen of the mouse. When the tumor volume grew to

50-100 $mm^3$, the DiR-labeled MPEG-PLH-VES and MPEG-PLH-VES/B NPs were intravenously dosed into the tumor-engrafted mice, respectively. The time-dependent biodistribution was imaged with an IVIS® Lumina II Imaging System at the designed time points. At last, the tumors and major organs were immediately excised and transferred for *ex vivo* imaging.

*2.13. In vivo tumor growth inhibition study*

Various formulations (including saline, free DOX solution, DOX-encapsulated MPEG-PLH-VES NPs and DOX-encapsulated MPEG-PLH-VES/B NPs) were intravenously dosed into the MCF-7/ADR tumor-engrafted mice every 3 days at the dose of 10 mg/kg DOX, respectively. Body weight and tumor volume (length × $width^2/2$, determined with a caliper) were recorded every other day. Finally, the mice were euthanized to isolate the tumors and hearts. the detailed experimental procedure for H&E staining was described in the supporting information.

*2.14. Statistical analysis*

Data were presented as mean ± SD. Statistical analysis were determined by the analysis of variance (ANOVA) for the group numbers exceeding 3 or Student's t-test between 2 groups. P values less than 0.05 were considered to be statistically significant.

## 3. RESULTS AND DISCUSSIONS

*3.1. Characterization of the synthesized polymers*

The synthesis routes of MPEG-PLH-VES and biotin-PEG-VES were illustrated in Figure 1. The MPEG-poly($N^{im}$-DNP-L-histidine) (protected MPEG-PLH) copolymer

was synthesized via the ring-opening polymerization of $N^{im}$-DNP-L-histidine carboxyanhydride using MPEG2000-$NH_2$ as a macroinitiator[49] (Figure 1A). The representative $^1$H NMR spectrum of protected MPEG-PLH exhibited a series of peaks at $\delta_a$ 3.49 ppm (−OC$\underline{H}_2$C$\underline{H}_2$O−), $\delta_b$ 7.79 ppm (−CO−N$\underline{H}$−), $\delta_k$ 4.24 ppm (−C$\underline{H}$−), $\delta_c$ 8.15 ppm (the proton "c" on the imidazole moiety) and $\delta_d$ 8.76 ppm (the proton "d" on the imidazole moiety). The peaks ($\delta_h$ 9.16 ppm; $\delta_i$ 8.78 ppm; $\delta_j$ 7.93 ppm) belonged to various moieties of phenyl group (DNP) (Figure 2A). The representative $^1$H NMR spectrum of MPEG-PLH-VES exhibited a series of peaks at $\delta_a$ 3.58 ppm (−OC$\underline{H}_2$C$\underline{H}_2$O−), $\delta_b$ 7.94 and 7.91 ppm (−CO−N$\underline{H}$−), $\delta_c$ 8.44 ppm (the proton "c" on the imidazole moiety), $\delta_d$ 8.87 ppm (the proton "d" on the imidazole moiety) (Figure 2B). The peaks in the aliphatic region ($\delta_e$ 2.00 and 1.90 ppm; $\delta_f$ 1.75 ppm; $\delta_g$ 0.85 ppm) could be assigned to the protons of vitamin E tail. As opposed to the spectrum in Fig.2A, the disappearance of the characteristic peaks ($\delta_h$, $\delta_i$ and $\delta_j$) of the phenyl protons on DNP group indicated that the DNP protection groups were successfully deprotected (Figure 2B). The representative $^1$H NMR spectrum of biotin-PEG-VES exhibited a series of peaks at $\delta_a$ 6.35 and 6.41 ppm (the proton "a" on the biotin moiety), $\delta_b$ 4.13 and 4.30 ppm (the proton "b" on the biotin moiety), $\delta_d$ 7.83 and 7.91 ppm (−CO−N$\underline{H}$−), $\delta_e$ 3.51 ppm (−OC$\underline{H}_2$C$\underline{H}_2$O−), and the characteristic peaks of VES moiety (Figure S1).

The GPC measurement confirmed the peak of MPEG-PLH-VES at 33.23 min and biotin-PEG-VES at 31.04 min, respectively (Figure 3A). All of the synthesized polymers showed well-defined unimodal distribution (PDI <1.2) (Figure 3A, table S1).

Pertaining to the biotin-PEG-VES conjugate, the molecular weight ($M_w$) measured by GPC was relatively higher than $M_n$ by $^1$H-NMR measurement (Table S1). Indeed, the molecular weights based on GPC (size-exclusion chromatography) reflect the molecular size of the tested compounds in solution, which is often influenced by the specific molecular conformation in the solution[34, 50]. To this respect, the molecular weight of the synthesized polymer calculated from the $^1$H-NMR spectra was utilized in this work.

*3.2. Acid–base titration of MPEG-PLH-VES*

The acid–base titration method was employed to assess the pKa and buffering capacity of the MPEG-PLH-VES copolymer (Figure 3B). The copolymer exhibited an appreciable buffering capacity in physiological pH range from 5.0 to pH 8.0. The apparent pKa of the MPEG-PLH-VES polymer was determined to be approximate 6.67 in terms of the first-order derivation of the titration profile, consistent with previous report[51]. The observed buffering capacity was believed to be attributable to the PLH segment contained in the MPEG-PLH-VES copolymer. Along pH gradient from neutral milieu to acidic milieu, the imidazole rings of PLH segment were capable of progressively binding protons to induce the change of hydrophobicity of the MPEG-PLH-VES copolymer[52]. Such a pH-responsive amphoteric property of PLH block is essential for the pH-sensitive function of the MPEG-PLH-VES copolymer.

*3.3. pH-induced particle size and PDI variation*

The particle size and PDI variation of the MPEG-PLH-VES polymeric NPs in

response to pH gradient was recorded by DLS measurement (Figure 3C). The average particle size and PDI value remained almost unchanged at pH 8.0 and 7.4. Stepwise adjustment of the pH of the sample solution (MPEG-PLH-VES NPs) at pH of 6.5, 6.0 and 5.0, resulted in consistent increase in average size, characterized with a linear slope of -56.9 nm/pH unit ($R^2$ = 0.9968). Meanwhile, the PDI value of the MPEG-PLH-VES also increased (from 0.137 to 0.250) in response to pH gradient from 7.4 to 5.0. In pertinent to the MPEG-PLH-VES NPs, the associative hydrophobic force of VES moieties and deprotonated PLH segments strengthened the inner core structure under neutral pH milieu. Along pH decrease of the sample solution, the gradual protonation of the imidazole groups in PLH segments enabled PLH undergoing a hydrophobic to hydrophilic transition, wherein the electrostatic repulsive force also progressively generated. This molecular transformation, eventually accounts for the structural destabilization, evidenced as the swelling or aggregation of NPs[33].

*3.4. Characterization of DOX-encapsulated polymeric NPs*

The physical characterizations of the DOX-encapsulated polymeric NPs were summarized in Table 1. The DOX-encapsulated NPs were determined to possess similar DLS size at approximate 130 nm with unimodal distribution of PDI below 0.2 (Figure 3E and Figure S 2B). Biotin decoration appeared to not affect the size and size distribution of the DOX-encapsulated polymeric NPs. TEM morphology characterization revealed that the drug-encapsulated NPs with or without biotin decoration exhibited nanoscaled spherical formation (Figure 3D and Figure S2A). The

relative smaller size observed via TEM as compared to DLS measurement may be ascribed to the shrinkage of the nanoparticles during drying in the TEM sample preparation[53]. The zeta potential was measured to be -5.82 mV for DOX-loaded MPEG-PLH-VES NPs and -2.98 mV for MPEG-PLH-VES/B NPs, respectively. The low absolute value of the zeta potential of the polymeric NPs may be attributed to the existence of the neutrally charged PLH segments near the nanoparticle surface and the spatial charge shielding effect of PEG chains[19, 54]. In addition, Both DOX-loaded MPEG-PLH-VES NPs and MPEG-PLH-VES/B NPs were determined to possess appreciable drug EE, 90.69 ± 2.63% and 89.53 ± 3.77%, respectively.

*3.5. In vitro drug release*

The *in vitro* drug release behaviors of the DOX-loaded MPEG-PLH-VES NPs and MPEG-PLH-VES/B NPs were investigated in two dissolution media (pH 5.0 and 7.4) at 37 °C (Figure 3F). Overall, the DOX release from MPEG-PLH-VES NPs was not affected by the biotin decoration. Yet, the DOX-loaded polymeric NPs displayed apparent pH-dependent drug release behavior, as evidenced by the faster DOX release at endo-lysosomal pH (~5.0). In pH 7.4 releasing media, both MPEG-PLH-VES NPs and MPEG-PLH-VES/B NPs had a low cumulative drug release around 30% within 72 h. In contrast, as the pH decreased to 5.0, the cumulative DOX release percentage was increased to 72.1% for MPEG-PLH-VES NPs and 70.2% for MPEG-PLH-VES/B NPs, respectively ($P > 0.05$). This result may be attributed to the protonation of DOX and PLH segments under acidic condition. Along pH gradient from pH 7.4 to 5.0, the protonated PLH segments conduced to the swelling of micellar hydrophobic core due

to the strengthening of electrostatic repulsion. Moreover, the dissociation of doxorubicin was also enhanced with the decrease of pH, leading to a higher solubility in aqueous solution and weaker hydrophobic interaction with the inner core building blocks of VES-PLH. Meanwhile, the electrostatic repulsion between DOX molecules and PLH segments was also strengthened to further prompt the drug release from the polymeric nanocarriers[55].

*3.6. Assay of P-gp expression, mitochondrial membrane potential and ATP level*

To study the plausible mechanisms of reversing MDR, the impact of the MPEG-PLH-VES or TPGS on the P-gp expression level of the MCF-7/ADR cells was initially investigated using fluorescently labeled antibody. The TPGS and MPEG-PLH-VES did not induce a significant alteration on fluorescence intensity of MCF7/ADR cells as compared to corresponding mean value in the control group (Figure 4A). It indicates that the inhibition on the expression level of P-gp is not involved in the reversal of MDR by MPEG-PLH-VES or TPGS[52]. The impact of the MPEG-PLH-VES or TPGS on the mitochondrial membrane potential ($\Delta\Psi_m$) of the MCF-7/ADR cells was then investigated based on a potential-dependent accumulation of JC-1 dye. This dye was characterized to enter selectively into mitochondria and undergo the red-shift in its emission from green (530 nm) to red (590 nm) as a consequence of the reversible formation of JC-1 aggregates based on membrane polarization. Hence, a reduced index of red/green fluorescence intensity represents the depolarizing behavior of the mitochondrial membrane. The index of JC-1 red/green of MCF-7/ADR cells exposed to MPEG-PLH-VES was determined to be merely 20.3%

relative to that of the control cells, lower than that of TPGS group (68.6% of control) ($P<0.01$, Figure 4B). It is well acknowledged that mitochondria are responsible for providing cells with usable energy. Therefore, the intracellular ATP level of MCF-7/ADR cells was also measured using a luciferin/luciferase assay. The MCF-7/ADR cells incubated with the blank medium were employed as a control. TPGS and MPEG-PLH-VES brought about a significant reduction of intracellular ATP level in MCF7/ADR cells to 34.4% and 84.4% relative to the control at 2 h post incubation, respectively (Figure 4C). In consistent with the change in mitochondrial membrane potential, the MPEG-PLH-VES also displayed a higher depletion of the intracellular ATP level as compared to TPGS ($p<0.01$). Most likely, vitamin E succinate (VES) and its analogues could induce cell apoptosis by interference of the ubiquinone-binding sites in mitochondrial respiratory complex II[56]. This behavior would disrupt the electron flux, and consequently induce destabilization onto the mitochondrial membrane. Meanwhile, the protonated PLH segment of MPEG-PLH-VES under acidic condition was believed to interact with the membrane components of the mitochondrial compartments, which may induce further loss of mitochondrial membrane potential. Such mitochondrial dysfunction hindered the ATP synthesis and resulted in the observed decrease in the intracellular ATP level[57]. P-gp is an ATP-dependent drug efflux transporter. Accordingly, the reduction in mitochondrial membrane potential and ATP level induced by MPEG-PLH-VES would exaggerate the inhibitory potency on P-gp mediated drug efflux, consequently bringing about the improved drug accumulation in drug-resistance tumor cells.

*3.7. Inhibition of P-gp ATPase*

The P-gp ATPase assay was carried out to explore the mechanism for P-gp inhibition by the MPEG-PLH-VES copolymer based on the P-gp-Glo™ assay system. Herein, $Na_3VO_4$ was selected as a specific inhibitor of P-gp. The samples treated with $Na_3VO_4$ possess no P-gp ATPase activity. Note that verapamil was selected as a P-gp substrate. It could stimulate the P-gp ATPase activity, leading to the ATP consumption. The corresponding assay employed an ATP-dependent luminescence reaction. The difference in luminescent signal (ΔRLU) between polymer treated-samples and $Na_3VO_4$-treated samples indicates the inhibition for P-gp ATPase activity by the test polymer, that is, the lower value of the ΔRLU, standing for the weaker activity of P-gp ATPase. Verapamil (50 μM) alone (control group) was capable of stimulating the P-gp ATPase activity by the specific binding of verapamil in the active center of P-gp, resulting in a significant ATP consumption (Figure 4D). In contrast, the MPEG-PLH-VES and TPGS distinctly inhibited the Verapamil-stimulated P-gp ATPase activity in a concentration-dependent manner. Moreover, the inhibition effect of verapamil-stimulated ATPase activity of P-gp by MPEG-PLH-VES was better than that by TPGS at the designed polymer concentrations (10 and 50 μM) ($P<0.01$, Figure 4D). A plausible reason for this promoted inhibitory activity may be as a result of the impact of varying the hydrophobe of TPGS by introducing the PLH segment[58]. In addition, plots of ΔRLU against the reciprocal concentration of verapamil exhibited a parallel trend among a class of MPEG-PLH-VES concentrations (Figure 4E). It indicates that MPEG-PLH-VES may not be a substrate of P-gp and not able to make

the competitive inhibition of substrate binding. This result is consistent with the previous investigations on TPGS and its analogues[10]. Similar to TPGS, MPEG-PLH-VES may inhibit ATPase inhibition through blocking substrate binding and/or P-gp allosteric modulation[19, 58].

*3.8. In vitro cytotoxicity*

The cytotoxic potency of DOX-encapsulated NPs together with the corresponding blank NPs was assessed in MCF-7 and MCF-7/ADR cells for 48 h incubation. The DOX solution was also assessed for comparison. Meanwhile, the cytotoxic profile of blank NPs was also assessed in L02 cells (human normal liver cells) for 48 h incubation, with the aim of verifying the selective cytotoxicity of blank NPs to the cancer cells. The cytotoxic activities of blank NPs (MPEG-PLH-VES NPs and blank MPEG-PLH-VES/B NPs) to MCF-7 cells were markedly higher than that to normal L02 cells at copolymer concentrations of 100 and 200 μg/mL ($P<0.01$) (Figure S3), suggesting that the blank NPs possess selective cytotoxicity to MCF-7 breast cancer cells. A plausible reason for the acquired anticancer effect could ascribe to the VES analogs in terms of down-regulating the antiapoptotic proteins of cancer cells or/and activating mitochondria-specific apoptotic pathways through the production of reactive oxygen species (ROS) within tumor cells [59]. In contrast, the normal cells were envisioned to be less susceptible to the aforementioned ROS-initiated apoptosis from the VES analogs due to their effective anti-oxidant defenses, thereby preventing further oxidative damage and cell death[60]. In addition, the cytotoxic impact of the blank NPs on MCF-7/ADR cells was observed to be lower than that of MCF-7 cells

(Figure 5 and Figure S3). This result was conjectured to be as a result of the strengthened antioxidant abilities of multidrug-resistant cancer cells (e.g.: activation of the antioxidant transcription factor Nrf2 or other ROS scavengers)[61].

Pertaining to the DOX formulations, free DOX solution exhibited relatively higher cytotoxic potency to the drug-sensitive MCF-7 cancer cells at all designed DOX concentrations as compared to the NPs of DOX-loaded MPEG-PLH-VES and MPEG-PLH-VES/B (Figure 5A). Free DOX solution was calculated to have an IC50 value of 0.3 μg/mL for MCF-7 cells, lower than those obtained for the DOX-loaded nanoparticulate formulations (IC50=2.3 μg/mL for MPEG-PLH-VES NPs and IC50=1.7 μg/mL for MPEG-PLH-VES/B NPs, respectively). The relative low inhibitory potency of nanoparticulate formulation as compared to molecular DOX was likely to be as a consequence of the relative retarded release of drug from the polymeric nanocarriers[62]. In contrast, free DOX molecules were able to be expeditiously internalized by sensitive MCF-7 cells with low expression of P-gp and readily localized inside the cancerous cells, accounting for high cytotoxicity as a result of the action of DOX with nucleus DNA in cancer cells[63, 64].

As opposed to the drug-vulnerable MCF-7 cancer cells, free DOX was observed to exert no significant cytotoxic potency to MCF-7/ADR cells over a concentration range of 2.5~40 μg/mL, likely due to the excessive expression of drug resistant P-gp (Figure 5B). By contrast, the constructed DOX-loaded nanoparticle formulations showed pronounced cytotoxic potency to MCF-7/ADR cells in a concentration-dependent manner. The IC50 value was calculated to be 11.1 and 8.6

μg/mL for DOX-loaded MPEG-PLH-VES NPs and MPEG-PLH-VES/B NPs, respectively. DOX-loaded MPEG-PLH-VES/B NPs was determined to be approximate 1.3-times as effective as DOX-loaded MPEG-PLH-VES NPs. The MDR-reversing mechanisms of the constructed nanoparticle formulations may involve the following factors: firstly, the entrapment of DOX molecules in the polymeric NPs were internalized through endocytosis pathway, thereby evading MDR efflux pumps; secondly, the MPEG-PLH-VES, as a TPGS analog, has been validated in correlation of the inhibition of Verapamil-induced P-gp ATPase activity; thirdly, the MPEG-PLH-VES copolymer could induce the loss of the mitochondrial membrane potential and ATP level of MCF-7/ADR cells, accounting for further inhibition of the P-gp mediated drug efflux; lastly, the strategic biotin-functionalized formation could augment the intracellular drug concentration by mean of the biotin receptor-mediated endocytosis of the NPs to further exaggerate the cell death to the affected MCF-7/ADR cells.

*3.9. Cellular uptake and intracellular distribution*

The cellular uptake activities of DOX solution and diverse DOX-loaded NPs in MCF-7/ADR cells were quantitatively analyzed with flow cytometry. The cellular uptake of the DOX-loaded nanoparticulate formulations exhibited a distinct time-dependent manner (Figure 6). The fluorescence intensity of the internalized DOX at 4 h post incubation was higher than that at 1 h post incubation ($p < 0.01$). Of note, the intracellular drug fluorescence intensities with the aids of nanoparticle formulations at 1 and 4 h post incubation were markedly higher than that of DOX

solution ($p < 0.01$). Particularly, the DOX-encapsulated MPEG-PLH-VES/B NPs led to 4.52- and 4.88-fold higher cellular uptake than the DOX solution, and 1.39- and 1.52-fold higher cellular uptake than the drug-encapsulated MPEG-PLH-VES NPs at 1 h and 4 h post incubation, respectively (Figure 6C). It suggests the possibility of endocytosis of DOX-loaded polymeric NPs by evading P-gp-mediated efflux of drug-resistance cancerous cells, accounting for increased cellular internalization. Moreover, the interaction between biotin moiety and its receptors over-expressed on the surface of the cancerous cells was believed to further improve the cellular uptake efficiency of MPEG-PLH-VES NPs[47, 65].

The intracellular distribution of drug-loaded NPs in MCF-7/ADR cells was investigated with CLSM. The endo-lysosomes and nuclei were labeled with LysoTracker DND-26 (green) and Hoechst 33258 (blue), respectively. In principle, yellow pixels in the CLSM image stand for the colocalization of DOX (red) and endo-lysosomes (green). As shown in Figure 7, the internalized DOX (sum of yellow and red pixels) were observed as yellow for both DOX-loaded MPEG-PLH-VES NPs and MPEG-PLH-VES/B NPs treated cells at 1 h post incubation. This implied that the drug-encapsulated NPs were internalized into the cancerous cells via the endocytosis pathway and subsequently localized in the endo-lysosome compartments. In contrast, after 4 h incubation, the population of red pixels was observed to significantly increase in the cytoplasm as companied with reduced population of yellow pixels, suggesting an effective endo-lysosomal escape of DOX. This result can be possibly explained by the facilitated protonation of PLH component (proton sponge effect) of

the MPEG-PLH-VES copolymer in the acidic endo-lysosome compartments, conducing to sequential endo-lysosome osmotic swelling, disruption of the endo-lysosome membrane and cytoplasmic translocation of DOX[33]. Such facilitated endo-lysosomal escape by MPEG-PLH-VES copolymer was believed to be crucial in inhibiting the DOX exocytosis via the endo-lysosomal system or avoiding DOX degradation in the endo-lysosomal compartments, eventually leading to the low drug elimination of cancerous cells.

*3.10. In vivo imaging*

A whole-body NIR imaging system was utilized to visualize the biodistribution of DiR-loaded MPEG-PLH-VES NPs and MPEG-PLH-VES/B NPs in the MCF-7/ADR tumor-engrafted nude mice (Figure 8A). Herein, DiR was employed as a near-infrared fluorescence probe with respect to its advantageous long-wavelength excitation and emission for deep light penetration and low auto-fluorescence interference[66]. The dye loading efficiency and encapsulation efficiency of DiR-loaded NPs were approximate 2% and 100%, respectively. The *in vitro* dye leakage profiles of DiR-loaded NPs were investigated in pH 7.4 releasing media at 37 ℃ using dialysis method. No leakage of DiR was detected from polymeric NPs within 48 h, suggesting that the florescence of DiR could be utilized to evaluate the *in vivo* distribution activities of MPEG-PLH-VES NPs and MPEG-PLH-VES/B NPs. At 2 h post administration, the loaded DiR molecules were abundantly localized in the livers and the accumulation in the tumors was limited for both MPEG-PLH-VES NPs and MPEG-PLH-VES/B NPs. Nevertheless, the fluorescence intensity in the tumors appeared to gradually increase

over time. Marked fluorescence accumulation in the tumors was validated at 12 h post administration of both MPEG-PLH-VES and MPEG-PLH-VES/B NPs. Moreover, the MPEG-PLH-VES/B NPs exhibited more intensive fluorescence signals in tumor tissue as compared to MPEG-PLH-VES NPs. Meanwhile, the *ex vivo* fluorescent images of the dissected tumors reconfirmed the higher tumor accumulation of MPEG-PLH-VES/B NPs compared to MPEG-PLH-VES NPs (Figure 8B). Considerable liver and spleen accumulation was observed for the two DiR-loaded NPs, which is believed to be attributable to the nonspecific capture by the reticuloendothelial system residing in the livers and spleens.

*3.11. In vivo tumor growth suppression*

The ability of nanoparticulate formulations to reverse MDR was evaluated in mice bearing the subcutaneous MCF-7/ADR tumor xenografts. The saline group served as the control group. DOX solution group exhibited a limited tumor inhibitory activity (an average 29.4% reduction in tumor volume compared to the saline group) on account of drug resistant characteristics of MCF-7/ADR cells (Figure 9A). By contrast, all DOX-loaded nanoparticle formulations exhibited high *in vivo* antitumor efficacy at the end of 13 days. Of note, the tumor volume of the mice treated with MPEG-PLH-VES/B group was calculated to be 27.4% relative to that of the control group, lower than that of MPEG-PLH-VES group (42.2%) ($p < 0.05$), indicating the strategic use of MPEG-PLH-VES and biotin-PEG-VES for pursuit of systemic tumor growth suppression (Figure 9A and B). The pathology analysis of the post-treated tumor tissues was further conducted with H&E staining (Figure 9D). The tumor

sections collected from DOX-loaded nanoparticle formulations treatment groups (especially for DOX-loaded MPEG-PLH-VES/B) showed extensive hemorrhagic inflammation and severe spotty necrosis compared with that collected from free DOX solution treatment group. The improved antitumor efficacy of MPEG-PLH-VES/B group might be due to the synergistic outcomes of passive (EPR effect-mediated) tumor targeting and active (biotin-mediated) tumor targeting.

The average body weight of every group was also recorded to assess the overall systemic toxicity. The saline control group showed a moderate increase in body weight due to no drug intervention. In contrast, ~30% loss relative to the initial body weight was confirmed for the mice treated with free DOX solution group at the end of animal test. By comparision, the body weight change of the DOX-loaded nanoparticle formulations groups was negligible, demonstrating a low degree of systemic toxicity (Figure 9C). The H&E staining for the cross-section of heart sections further affirmed the associated cardiotoxicity of the diverse DOX formulations (Figure 9D). Pertaining to the specimen derived from the free DOX solution, apparent cardiac tissue damages (such as cytoplasmic vacuolization, myocardial fiber breakage and disarray) were observed, consistent with the previously documented result of severe cardiotoxicity from free DOX solution[15, 67]. By comparison, no severe cardiac tissue damage was confirmed for the mice treated with DOX-encapsulated nanoparticle formulations, verifying that nanoparticle formulations of DOX can afford a tempting merit of reduced systemic cardiotoxicity. Hence, the investigation from DOX-based therapeutics functionalized with the MPEG-PLH-VES/B nanocarriers suggests

intriguing aspects of both potency and safety profile in the treatment of MCF-7/ADR tumor-engrafted mice.

## 4. CONCLUSIONS

In summary, as a proof of principle, we have designed a multifunctional drug delivery system (MPEG-PLH-VES/B NPs) with the aim of overcoming MDR. MPEG-PLH-VES had no influence on P-gp expression of MCF-7/ADR but exhibited a significant influence on the loss of mitochondrial membrane potential, the depletion of intracellular ATP level and the inhibition of P-gp ATPase activity of MCF-7/ADR cells. The DOX-loaded MPEG-PLH-VES/B NPs entitled efficient DOX cellular uptake into MCF-7/ADR cells, pH-dependent drug release, PLH facilitated endo-lysosomal escape, high cytotoxicity against MCF-7/ADR cells, selective tumor accumulation in a MCF-7/ADR xenograft tumor model and evident inhibition on tumor growth. The obtained results portend the intriguing potential of MPEG-PLH-VES/B nanocarriers for overcoming MDR in cancer chemotherapy.

## Supporting Information

Molecular weights of synthesized polymers; typical $^{1}$H-NMR spectra of biotin-PEG-VES; TEM image and size distribution of DOX-loaded MPEG-PLH-VES/B NPs; in vitro cytotoxicity of blank NPs against L02, MCF-7 and MCF-7/ADR cells after treatment for 48 h.

## Conflict of interest

The authors declare no conflicts of interest.

## Acknowledgements

This project was partly supported by the Natural Science Foundation of China (No: 81302713 and 81703432).

## References

1. Iyer, A. K.; Singh, A.; Ganta, S.; Amiji, M. M., Role of integrated cancer nanomedicine in overcoming drug resistance. *Adv Drug Deliv Rev* **2013,** 65, (13-14), 1784-802.

2. Livney, Y. D.; Assaraf, Y. G., Rationally designed nanovehicles to overcome cancer chemoresistance. *Adv Drug Deliv Rev* **2013,** 65, (13-14), 1716-30.

3. Yan, X.; Yu, Q.; Guo, L.; Guo, W.; Guan, S.; Tang, H.; Lin, S.; Gan, Z., Positively Charged Combinatory Drug Delivery Systems against Multi-Drug-Resistant Breast Cancer: Beyond the Drug Combination. *ACS Appl Mater Interfaces* **2017,** 9, (8), 6804-6815.

4. Chen, Z.; Shi, T.; Zhang, L.; Zhu, P.; Deng, M.; Huang, C.; Hu, T.; Jiang, L.; Li, J., Mammalian drug efflux transporters of the ATP binding cassette (ABC) family in multidrug resistance: A review of the past decade. *Cancer Lett* **2016,** 370, (1), 153-64.

5. Gottesman, M. M.; Fojo, T.; Bates, S. E., Multidrug resistance in cancer: role of ATP-dependent transporters. *Nat Rev Cancer* **2002,** 2, (1), 48-58.

6. Liu, Y.; Fang, J.; Joo, K. I.; Wong, M. K.; Wang, P., Codelivery of chemotherapeutics via crosslinked multilamellar liposomal vesicles to overcome multidrug resistance in tumor. *PLoS One* **2014,** 9, (10), e110611.

7. Zhao, Y.; Chen, F.; Pan, Y.; Li, Z.; Xue, X.; Okeke, C. I.; Wang, Y.; Li, C.; Peng, L.; Wang, P. C.; Ma, X.; Liang, X. J., Nanodrug Formed by Coassembly of Dual Anticancer Drugs to Inhibit Cancer Cell Drug Resistance. *ACS Appl Mater Interfaces* **2015,** 7, (34), 19295-305.

8. Battistella, C.; Klok, H. A., Reversion of P-gp-Mediated Drug Resistance in Ovarian Carcinoma Cells with PHPMA-Zosuquidar Conjugates. *Biomacromolecules* **2017,** 18, (6), 1855-1865.

9. Chavanpatil, M. D.; Patil, Y.; Panyam, J., Susceptibility of nanoparticle-encapsulated paclitaxel to P-glycoprotein-mediated drug efflux. *Int J Pharm* **2006,** 320, (1-2), 150-6.

10. Wang, J.; Sun, J.; Chen, Q.; Gao, Y.; Li, L.; Li, H.; Leng, D.; Wang, Y.; Sun, Y.; Jing, Y.; Wang, S.; He, Z., Star-shape copolymer of lysine-linked di-tocopherol polyethylene glycol 2000 succinate for doxorubicin delivery with reversal of multidrug resistance. *Biomaterials* **2012,** 33, (28), 6877-88.

11. Guo, Y.; Luo, J.; Tan, S.; Otieno, B. O.; Zhang, Z., The applications of Vitamin E TPGS in drug delivery. *Eur J Pharm Sci* **2013,** 49, (2), 175-86.

12. Tang, J.; Fu, Q.; Wang, Y.; Racette, K.; Wang, D.; Liu, F., Vitamin E reverses multidrug resistance in vitro and in vivo. *Cancer Lett* **2013,** 336, (1), 149-57.

13. Zhang, Z.; Tan, S.; Feng, S. S., Vitamin E TPGS as a molecular biomaterial for drug delivery. *Biomaterials* **2012,** 33, (19), 4889-906.

14. Muthu, M. S.; Kulkarni, S. A.; Liu, Y.; Feng, S. S., Development of docetaxel-loaded vitamin E TPGS micelles: formulation optimization, effects on brain cancer cells and biodistribution in rats. *Nanomedicine (Lond)* **2012,** 7, (3), 353-64.

15. Tuguntaev, R. G.; Chen, S.; Eltahan, A. S.; Mozhi, A.; Jin, S.; Zhang, J.; Li, C.; Wang, P. C.; Liang, X. J., P-gp Inhibition and Mitochondrial Impairment by Dual-Functional Nanostructure Based on Vitamin E Derivatives To Overcome

Multidrug Resistance. *ACS Appl Mater Interfaces* **2017,** 9, (20), 16900-16912.

16. Mi, Y.; Liu, Y.; Feng, S. S., Formulation of Docetaxel by folic acid-conjugated d-alpha-tocopheryl polyethylene glycol succinate 2000 (Vitamin E TPGS(2k)) micelles for targeted and synergistic chemotherapy. *Biomaterials* **2011,** 32, (16), 4058-66.

17. Lu, J.; Huang, Y.; Zhao, W.; Chen, Y.; Li, J.; Gao, X.; Venkataramanan, R.; Li, S., Design and characterization of PEG-derivatized vitamin E as a nanomicellar formulation for delivery of paclitaxel. *Mol Pharm* **2013,** 10, (8), 2880-90.

18. Lu, J.; Zhao, W.; Liu, H.; Marquez, R.; Huang, Y.; Zhang, Y.; Li, J.; Xie, W.; Venkataramanan, R.; Xu, L.; Li, S., An improved D-alpha-tocopherol-based nanocarrier for targeted delivery of doxorubicin with reversal of multidrug resistance. *J Control Release* **2014,** 196, 272-86.

19. Hao, T.; Chen, D.; Liu, K.; Qi, Y.; Tian, Y.; Sun, P.; Liu, Y.; Li, Z., Micelles of d-alpha-Tocopheryl Polyethylene Glycol 2000 Succinate (TPGS 2K) for Doxorubicin Delivery with Reversal of Multidrug Resistance. *ACS Appl Mater Interfaces* **2015,** 7, (32), 18064-75.

20. Xu, P.; Meng, Q.; Sun, H.; Yin, Q.; Yu, H.; Zhang, Z.; Cao, M.; Zhang, Y.; Li, Y., Shrapnel nanoparticles loading docetaxel inhibit metastasis and growth of breast cancer. *Biomaterials* **2015,** 64, 10-20.

21. Liu, Y.; Rohrs, J.; Wang, P., Advances and challenges in the use of nanoparticles to optimize PK/PD interactions of combined anti-cancer therapies. *Curr Drug Metab* **2014,** 15, (8), 818-28.

22. Cao, Y.; Yi, J.; Yang, X.; Liu, L.; Yu, C.; Huang, Y.; Sun, L.; Bao, Y.; Li, Y., Efficient Cancer Regression by a Thermosensitive Liposome for Photoacoustic Imaging-Guided Photothermal/Chemo Combinatorial Therapy. *Biomacromolecules* **2017,** 18, (8), 2306-2314.

23. Zhu, H.; Chen, H.; Zeng, X.; Wang, Z.; Zhang, X.; Wu, Y.; Gao, Y.; Zhang, J.; Liu, K.; Liu, R.; Cai, L.; Mei, L.; Feng, S. S., Co-delivery of chemotherapeutic drugs with vitamin E TPGS by porous PLGA nanoparticles for enhanced chemotherapy against multi-drug resistance. *Biomaterials* **2014,** 35, (7), 2391-400.

24. Tian, J.; Xu, L.; Xue, Y.; Jiang, X.; Zhang, W., Enhancing Photochemical Internalization of DOX through a Porphyrin-based Amphiphilic Block Copolymer. *Biomacromolecules* **2017,** 18, (12), 3992-4001.

25. Chiang, W. L.; Ke, C. J.; Liao, Z. X.; Chen, S. Y.; Chen, F. R.; Tsai, C. Y.; Xia, Y.; Sung, H. W., Pulsatile drug release from PLGA hollow microspheres by controlling the permeability of their walls with a magnetic field. *Small* **2012,** 8, (23), 3584-8.

26. Xiao, H.; Noble, G. T.; Stefanick, J. F.; Qi, R.; Kiziltepe, T.; Jing, X.; Bilgicer, B., Photosensitive Pt(IV)-azide prodrug-loaded nanoparticles exhibit controlled drug release and enhanced efficacy in vivo. *J Control Release* **2014,** 173, 11-7.

27. Wang, Z.; Luo, T.; Sheng, R.; Li, H.; Sun, J.; Cao, A., Amphiphilic Diblock Terpolymer PMAgala-b-P(MAA-co-MAChol)s with Attached Galactose and Cholesterol Grafts and Their Intracellular pH-Responsive Doxorubicin Delivery. *Biomacromolecules* **2016,** 17, (1), 98-110.

28. Chen, J.; Ding, J.; Xu, W.; Sun, T.; Xiao, H.; Zhuang, X.; Chen, X., Receptor and

Microenvironment Dual-Recognizable Nanogel for Targeted Chemotherapy of Highly Metastatic Malignancy. *Nano Lett* **2017,** 17, (7), 4526-4533.

29. Kuang, T.; Liu, Y.; Gong, T.; Peng, X.; Hu, X.; Yu, Z., Enzyme-responsive Nanoparticles for Anticancer Drug Delivery. *Current Nanoscience* **2016,** 12, (1), 38-46.

30. Wu, P.; Jia, Y.; Qu, F.; Sun, Y.; Wang, P.; Zhang, K.; Xu, C.; Liu, Q.; Wang, X., Ultrasound-Responsive Polymeric Micelles for Sonoporation-Assisted Site-Specific Therapeutic Action. *ACS Appl Mater Interfaces* **2017,** 9, (31), 25706-25716.

31. Lee, E. S.; Gao, Z.; Bae, Y. H., Recent progress in tumor pH targeting nanotechnology. *J Control Release* **2008,** 132, (3), 164-70.

32. Lee, E. S.; Na, K.; Bae, Y. H., Doxorubicin loaded pH-sensitive polymeric micelles for reversal of resistant MCF-7 tumor. *J Control Release* **2005,** 103, (2), 405-18.

33. Hong, W.; Chen, D.; Jia, L.; Gu, J.; Hu, H.; Zhao, X.; Qiao, M., Thermo- and pH-responsive copolymers based on PLGA-PEG-PLGA and poly(L-histidine): synthesis and in vitro characterization of copolymer micelles. *Acta Biomater* **2014,** 10, (3), 1259-71.

34. Li, Z.; Qiu, L.; Chen, Q.; Hao, T.; Qiao, M.; Zhao, H.; Zhang, J.; Hu, H.; Zhao, X.; Chen, D.; Mei, L., pH-sensitive nanoparticles of poly(L-histidine)-poly(lactide-co-glycolide)-tocopheryl polyethylene glycol succinate for anti-tumor drug delivery. *Acta Biomater* **2015,** 11, 137-50.

35. Gao, Z. G.; Tian, L.; Hu, J.; Park, I. S.; Bae, Y. H., Prevention of metastasis in a

4T1 murine breast cancer model by doxorubicin carried by folate conjugated pH sensitive polymeric micelles. *J Control Release* **2011,** 152, (1), 84-9.

36. Hu, J.; Miura, S.; Na, K.; Bae, Y. H., pH-responsive and charge shielded cationic micelle of poly(L-histidine)-block-short branched PEI for acidic cancer treatment. *J Control Release* **2013,** 172, (1), 69-76.

37. Wang, J.; Wang, H.; Li, J.; Liu, Z.; Xie, H.; Wei, X.; Lu, D.; Zhuang, R.; Xu, X.; Zheng, S., iRGD-Decorated Polymeric Nanoparticles for the Efficient Delivery of Vandetanib to Hepatocellular Carcinoma: Preparation and in Vitro and in Vivo Evaluation. *ACS Appl Mater Interfaces* **2016,** 8, (30), 19228-37.

38. Yang, Y.; Wang, X.; Liao, G.; Liu, X.; Chen, Q.; Li, H.; Lu, L.; Zhao, P.; Yu, Z., iRGD-decorated red shift emissive carbon nanodots for tumor targeting fluorescence imaging. *J Colloid Interface Sci* **2017,** 509, 515-521.

39. Zhuang, Y.; Deng, H.; Su, Y.; He, L.; Wang, R.; Tong, G.; He, D.; Zhu, X., Aptamer-Functionalized and Backbone Redox-Responsive Hyperbranched Polymer for Targeted Drug Delivery in Cancer Therapy. *Biomacromolecules* **2016,** 17, (6), 2050-62.

40. Gao, Y. Y.; Chen, H.; Zhou, Y. Y.; Wang, L. T.; Hou, Y.; Xia, X. H.; Ding, Y., Intraorgan Targeting of Gold Conjugates for Precise Liver Cancer Treatment. *ACS Appl Mater Interfaces* **2017,** 9, (37), 31458-31468.

41. Russell-Jones, G.; McTavish, K.; McEwan, J.; Rice, J.; Nowotnik, D., Vitamin-mediated targeting as a potential mechanism to increase drug uptake by tumours. *J Inorg Biochem* **2004,** 98, (10), 1625-33.

42. Vadlapudi, A. D.; Vadlapatla, R. K.; Kwatra, D.; Earla, R.; Samanta, S. K.; Pal, D.; Mitra, A. K., Targeted lipid based drug conjugates: a novel strategy for drug delivery. *Int J Pharm* **2012,** 434, (1-2), 315-24.

43. Mitra, K.; Shettar, A.; Kondaiah, P.; Chakravarty, A. R., Biotinylated Platinum(II) Ferrocenylterpyridine Complexes for Targeted Photoinduced Cytotoxicity. *Inorg Chem* **2016,** 55, (11), 5612-22.

44. Lee, E. S.; Na, K.; Bae, Y. H., Super pH-sensitive multifunctional polymeric micelle. *Nano Lett* **2005,** 5, (2), 325-9.

45. Le Droumaguet, B.; Nicolas, J.; Brambilla, D.; Mura, S.; Maksimenko, A.; De Kimpe, L.; Salvati, E.; Zona, C.; Airoldi, C.; Canovi, M.; Gobbi, M.; Magali, N.; La Ferla, B.; Nicotra, F.; Scheper, W.; Flores, O.; Masserini, M.; Andrieux, K.; Couvreur, P., Versatile and efficient targeting using a single nanoparticulate platform: application to cancer and Alzheimer's disease. *ACS Nano* **2012,** 6, (7), 5866-79.

46. Guo, S.; Lv, L.; Shen, Y.; Hu, Z.; He, Q.; Chen, X., A nanoparticulate pre-chemosensitizer for efficacious chemotherapy of multidrug resistant breast cancer. *Sci Rep* **2016,** 6, 21459.

47. Yu, G.; Cook, T. R.; Li, Y.; Yan, X.; Wu, D.; Shao, L.; Shen, J.; Tang, G.; Huang, F.; Chen, X.; Stang, P. J., Tetraphenylethene-based highly emissive metallacage as a component of theranostic supramolecular nanoparticles. *Proc Natl Acad Sci U S A* **2016,** 113, (48), 13720-13725.

48. Zhang, W.; Wang, F.; Wang, Y.; Wang, J.; Yu, Y.; Guo, S.; Chen, R.; Zhou, D., pH and near-infrared light dual-stimuli responsive drug delivery using DNA-conjugated

gold nanorods for effective treatment of multidrug resistant cancer cells. *J Control Release* **2016,** 232, 9-19.

49. Liu, R.; He, B.; Li, D.; Lai, Y.; Tang, J. Z.; Gu, Z., Synthesis and characterization of poly(ethylene glycol)-b-poly( l -histidine)-b-poly( l -lactide) with pH-sensitivity. *Polymer* **2012,** 53, (7), 1473-1482.

50. Philipsen, H. J., Determination of chemical composition distributions in synthetic polymers. *J Chromatogr A* **2004,** 1037, (1-2), 329-50.

51. Lee, E. S.; Shin, H. J.; Na, K.; Bae, Y. H., Poly(L-histidine)-PEG block copolymer micelles and pH-induced destabilization. *J Control Release* **2003,** 90, (3), 363-74.

52. Qiu, L.; Qiao, M.; Chen, Q.; Tian, C.; Long, M.; Wang, M.; Li, Z.; Hu, W.; Li, G.; Cheng, L.; Cheng, L.; Hu, H.; Zhao, X.; Chen, D., Enhanced effect of pH-sensitive mixed copolymer micelles for overcoming multidrug resistance of doxorubicin. *Biomaterials* **2014,** 35, (37), 9877-9887.

53. Zhong, Y.; Yang, W.; Sun, H.; Cheng, R.; Meng, F.; Deng, C.; Zhong, Z., Ligand-directed reduction-sensitive shell-sheddable biodegradable micelles actively deliver doxorubicin into the nuclei of target cancer cells. *Biomacromolecules* **2013,** 14, (10), 3723-30.

54. Radovic-Moreno, A. F.; Lu, T. K.; Puscasu, V. A.; Yoon, C. J.; Langer, R.; Farokhzad, O. C., Surface charge-switching polymeric nanoparticles for bacterial cell wall-targeted delivery of antibiotics. *ACS Nano* **2012,** 6, (5), 4279-87.

55. Wei, T.; Liu, J.; Ma, H.; Cheng, Q.; Huang, Y.; Zhao, J.; Huo, S.; Xue, X.; Liang,

Z.; Liang, X. J., Functionalized nanoscale micelles improve drug delivery for cancer therapy in vitro and in vivo. *Nano Lett* **2013,** 13, (6), 2528-34.

56. Neuzil, J.; Dong, L. F.; Ramanathapuram, L.; Hahn, T.; Chladova, M.; Wang, X. F.; Zobalova, R.; Prochazka, L.; Gold, M.; Freeman, R.; Turanek, J.; Akporiaye, E. T.; Dyason, J. C.; Ralph, S. J., Vitamin E analogues as a novel group of mitocans: anti-cancer agents that act by targeting mitochondria. *Mol Aspects Med* **2007,** 28, (5-6), 607-45.

57. Wang, D. F.; Rong, W. T.; Lu, Y.; Hou, J.; Qi, S. S.; Xiao, Q.; Zhang, J.; You, J.; Yu, S. Q.; Xu, Q., TPGS2k/PLGA nanoparticles for overcoming multidrug resistance by interfering mitochondria of human alveolar adenocarcinoma cells. *ACS Appl Mater Interfaces* **2015,** 7, (7), 3888-901.

58. Wempe, M. F.; Wright, C.; Little, J. L.; Lightner, J. W.; Large, S. E.; Caflisch, G. B.; Buchanan, C. M.; Rice, P. J.; Wacher, V. J.; Ruble, K. M.; Edgar, K. J., Inhibiting efflux with novel non-ionic surfactants: Rational design based on vitamin E TPGS. *Int J Pharm* **2009,** 370, (1-2), 93-102.

59. Wang, A. T.; Liang, D. S.; Liu, Y. J.; Qi, X. R., Roles of ligand and TPGS of micelles in regulating internalization, penetration and accumulation against sensitive or resistant tumor and therapy for multidrug resistant tumors. *Biomaterials* **2015,** 53, 160-72.

60. Manda, G.; Isvoranu, G.; Comanescu, M. V.; Manea, A.; Debelec Butuner, B.; Korkmaz, K. S., The redox biology network in cancer pathophysiology and therapeutics. *Redox Biol* **2015,** 5, 347-57.

61. Glasauer, A.; Chandel, N. S., Targeting antioxidants for cancer therapy. *Biochem Pharmacol* **2014,** 92, (1), 90-101.

62. Wang, H.; Xie, H.; Wang, J.; Wu, J.; Ma, X.; Li, L.; Wei, X.; Ling, Q.; Song, P.; Zhou, L.; Xu, X.; Zheng, S., Self-Assembling Prodrugs by Precise Programming of Molecular Structures that Contribute Distinct Stability, Pharmacokinetics, and Antitumor Efficacy. *Advanced Functional Materials* **2015,** 25, (31), 4956-4965.

63. Duan, X.; Xiao, J.; Yin, Q.; Zhang, Z.; Yu, H.; Mao, S.; Li, Y., Smart pH-sensitive and temporal-controlled polymeric micelles for effective combination therapy of doxorubicin and disulfiram. *ACS Nano* **2013,** 7, (7), 5858-69.

64. Feng, X.-r.; Ding, J.-x.; Gref, R.; Chen, X.-s., Poly(β-cyclodextrin)-mediated polylactide-cholesterol stereocomplex micelles for controlled drug delivery. *Chinese Journal of Polymer Science* **2017,** 35, (6), 693-699.

65. Vadlapudi, A. D.; Vadlapatla, R. K.; Pal, D.; Mitra, A. K., Biotin uptake by T47D breast cancer cells: functional and molecular evidence of sodium-dependent multivitamin transporter (SMVT). *Int J Pharm* **2013,** 441, (1-2), 535-43.

66. Lu, J.; Chuan, X.; Zhang, H.; Dai, W.; Wang, X.; Wang, X.; Zhang, Q., Free paclitaxel loaded PEGylated-paclitaxel nanoparticles: preparation and comparison with other paclitaxel systems in vitro and in vivo. *Int J Pharm* **2014,** 471, (1-2), 525-35.

67. Cote, B.; Carlson, L. J.; Rao, D. A.; Alani, A. W. G., Combinatorial resveratrol and quercetin polymeric micelles mitigate doxorubicin induced cardiotoxicity in vitro and in vivo. *J Control Release* **2015,** 213, 128-133.

**Captions**

Table 1 Drug encapsulation efficiency (EE), size and zeta potential of DOX-loaded MPEG-PLH-VES NPs and MPEG-PLH-VES/B NPs.

Figure 1 The synthesis schemes of MPEG-PLH-VES copolymer and biotin-PEG-VES conjugate.

Figure 2 Typical $^{1}$H-NMR spectra of MPEG-poly($N^{im}$-DNP-L-histidine) (A) and MPEG-PLH-VES (B).

Figure 3 (A) Typical GPC chromatograms of MPEG-PLH-VES and biotin-PEG-VES. (B) Typical acid–base titration profile of MPEG-PLH-VES copolymer. (C) Particle size and PDI of MPEG-PLH-VES NPs at different pH values. (D) TEM image of DOX-loaded MPEG-PLH-VES NPs. (E) Size distribution of DOX-loaded MPEG-PLH-VES NPs measured using dynamic light scattering. (F) Release profiles of DOX-loaded MPEG-PLH-VES NPs and MPEG-PLH-VES/B NPs at different pH values.

Figure 4 The effects of MPEG-PLH-VES or TPGS on the P-gp expression (A), mitochondrial membrane potential (B) and intracellular ATP level (C) of MCF-7/ADR cells. Inhibitory effect of MPEG-PLH-VES or TPGS on verapamil-stimulated P-gp ATPase activity (D) and the uncompetitive inhibitory mechanism of P-gp ATPase by MPEG-PLH-VES (E). * indicates $p < 0.05$; ** indicates $p < 0.01$.

Figure 5 *In vitro* cytotoxicity of free DOX solution, DOX-loaded NPs and corresponding blank NPs against MCF-7 (A) and MCF-7/ADR (B) cancer cells after treatment for 48 h.

Figure 6 Flow cytometric histogram profiles of the intracellular uptake of DOX-loaded NPs and free DOX at 1 (A) and 4 h (B) in MCF-7/ADR cells and the fluorescence intensities of DOX accumulation after 1 and 4 h incubation (C). ** indicates $p < 0.01$.

Figure 7 CLSM images of DOX-loaded MPEG-PLH-VES NPs and MPEG-PLH-VES/B NPs in MCF-7/ADR cells after 1 and 4 h incubation. For each panel, images from left to right show DOX (red), lysosomes stained by Lysotracker (green), cell nuclei stained by Hoechst 33342 (blue) and overlay of all images. (Scale bar: 10 μm)

Figure 8 (A) *In vivo* imaging of MCF-7/ADR tumor-bearing nude mice injected with DiR-loaded MPEG-PLH-VES NPs and MPEG-PLH-VES/B NPs at 2, 4, 6, 8, 12 and 24 h post-injection, respectively. (B) *Ex vivo* imaging of DiR-loaded NPs in heart, liver, spleen, lung, kidney, and tumor of the nude mice bearing MCF-7/ADR tumor at 24 h post-injection, respectively.

Figure 9 (A) Changes of tumor volume after treatment with saline, free DOX solution, DOX-loaded MPEG-PLH-VES NPs and DOX-loaded MPEG-PLH-VES/B NPs in MCF-7/ADR tumor-bearing nude mice. (B) The photos of excised tumor tissue from MCF-7/ADR tumor-bearing nude mice at the time of sacrifice. (C) Body weight changes of MCF-7/ADR tumor-bearing nude mice after intravenous injection of saline, DOX solution and DOX-loaded NPs. (D) Images of H&E-stained heart and tumor sections harvested from the mice after treatment with saline, free DOX solution and DOX-loaded NPs.

Table 1 Drug encapsulation efficiency (EE), size and zeta potential of DOX-loaded MPEG-PLH-VES NPs and MPEG-PLH-VES/B NPs.

| Formulation | EE (%) | Particle size (nm) | Polydispersity | Zeta potential (mv) |
|---|---|---|---|---|
| MPEG-PLH-VES | 90.69 ± 2.63 | 130.2 ± 7.2 | 0.161 ± 0.017 | -5.82 ± 1.14 |
| MPEG-PLH-VES/B | 89.53 ± 3.77 | 126.0 ± 5.7 | 0.142 ± 0.011 | -2.98 ± 0.75 |

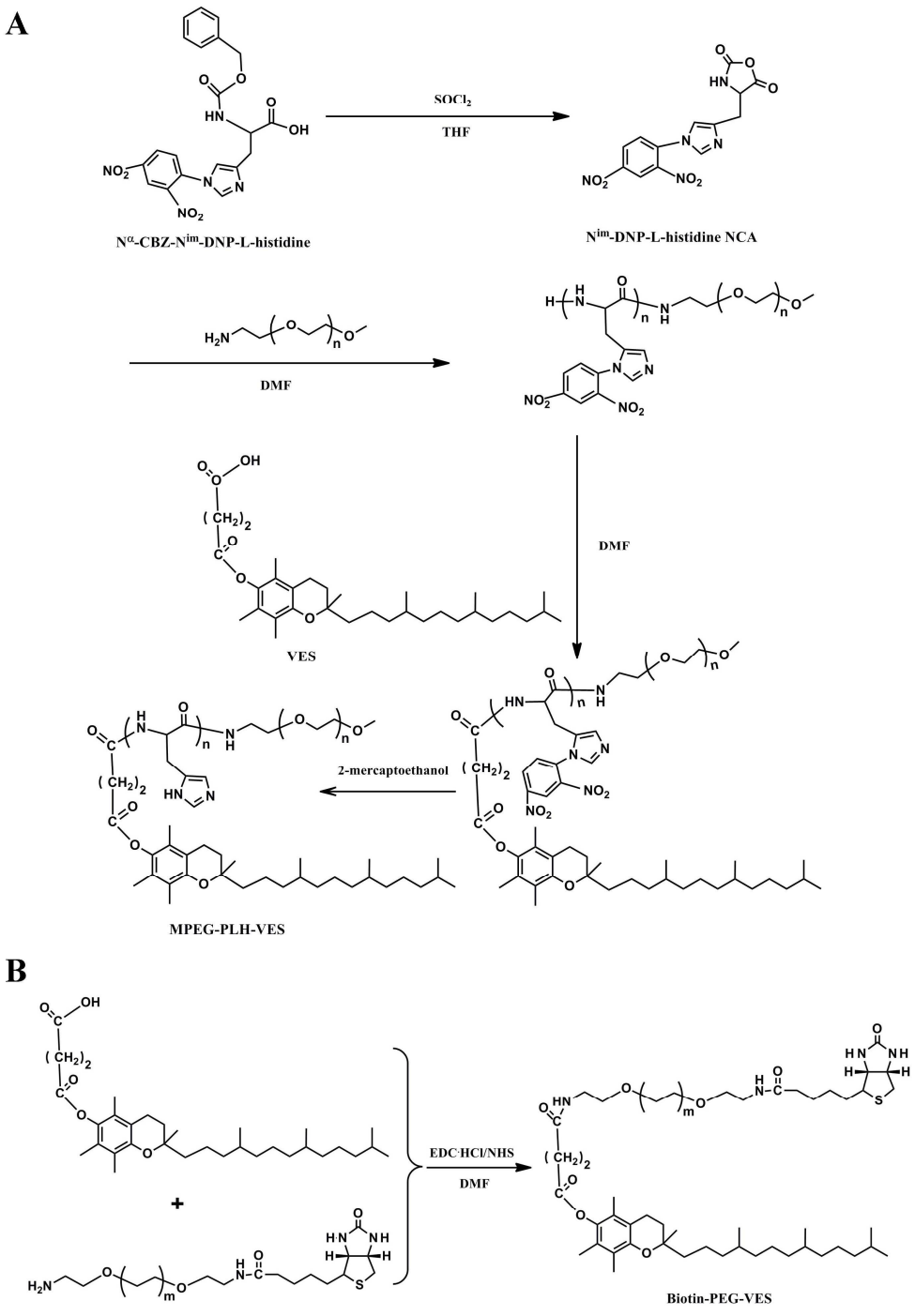


Figure 1 The synthesis schemes of MPEG-PLH-VES copolymer and biotin-PEG-VES conjugate.

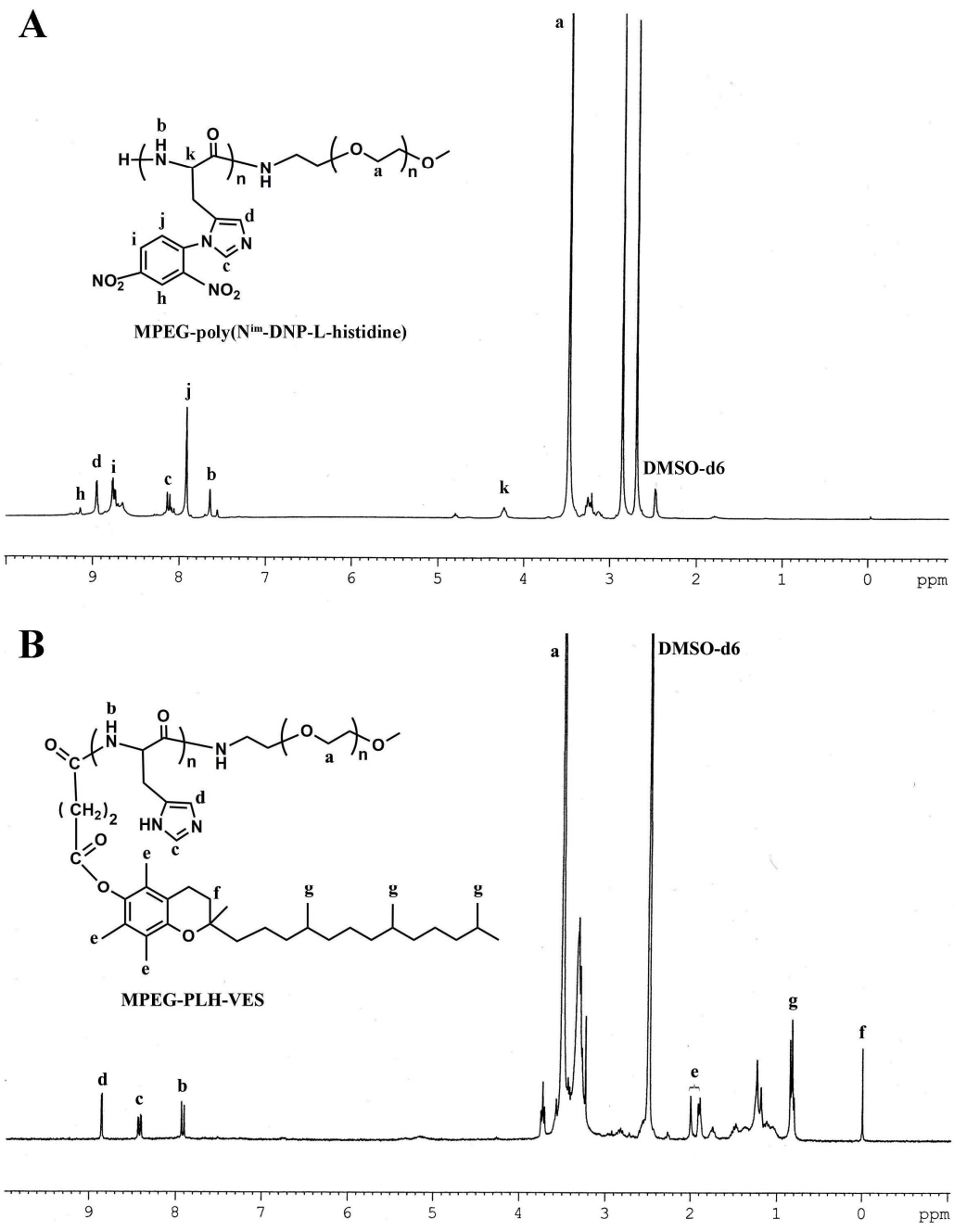


Figure 2 Typical $^{1}$H-NMR spectra of MPEG-poly($N^{im}$-DNP-L-histidine) (A) and MPEG-PLH-VES (B).

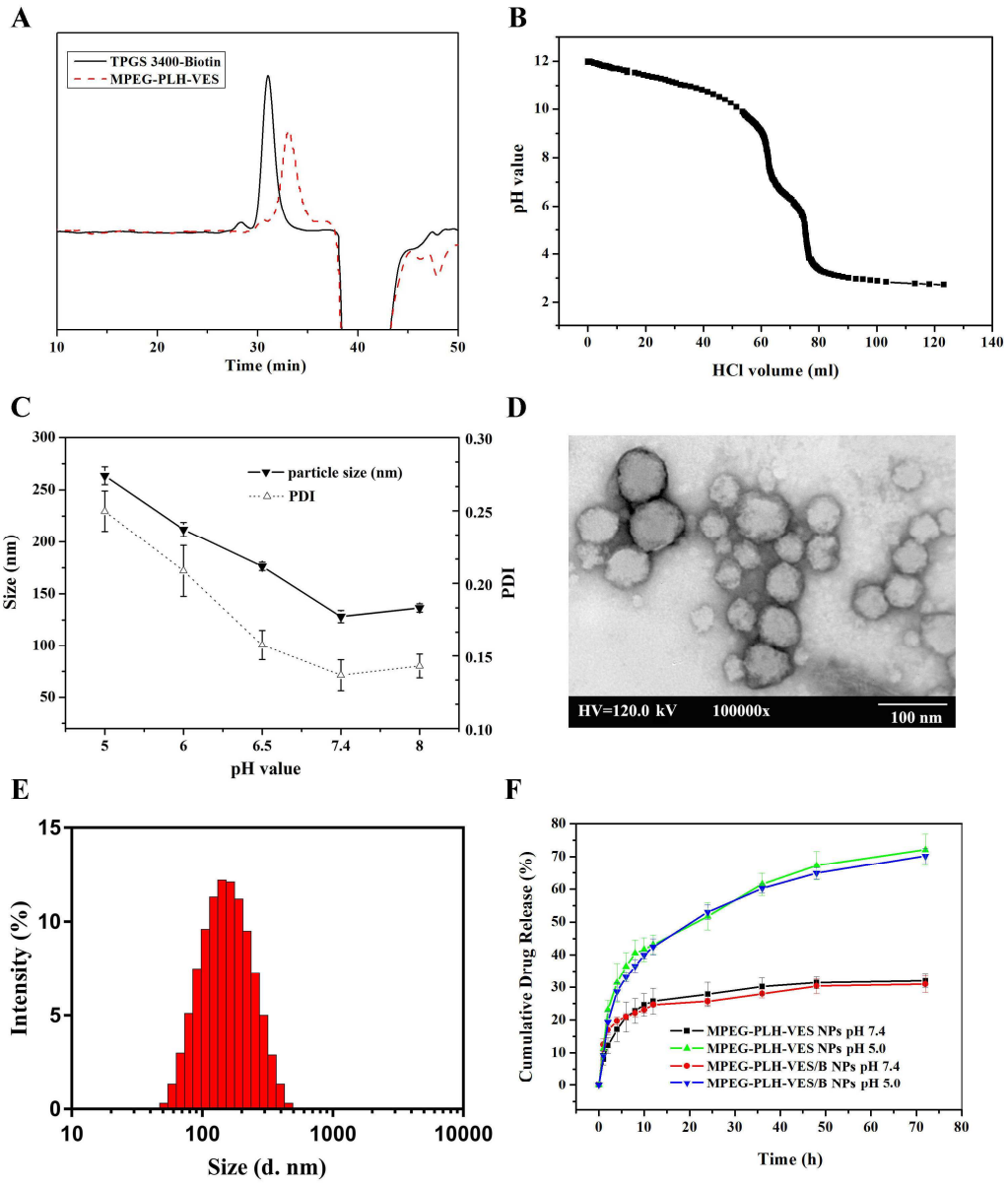


Figure 3 (A) Typical GPC chromatograms of MPEG-PLH-VES and biotin-PEG-VES. (B) Typical acid–base titration profile of MPEG-PLH-VES copolymer. (C) Particle size and PDI of MPEG-PLH-VES NPs at different pH values. (D) TEM image of DOX-loaded MPEG-PLH-VES NPs. (E) Size distribution of DOX-loaded MPEG-PLH-VES NPs measured using dynamic light scattering. (F) Release profiles of DOX-loaded MPEG-PLH-VES NPs and MPEG-PLH-VES/B NPs at different pH

values.

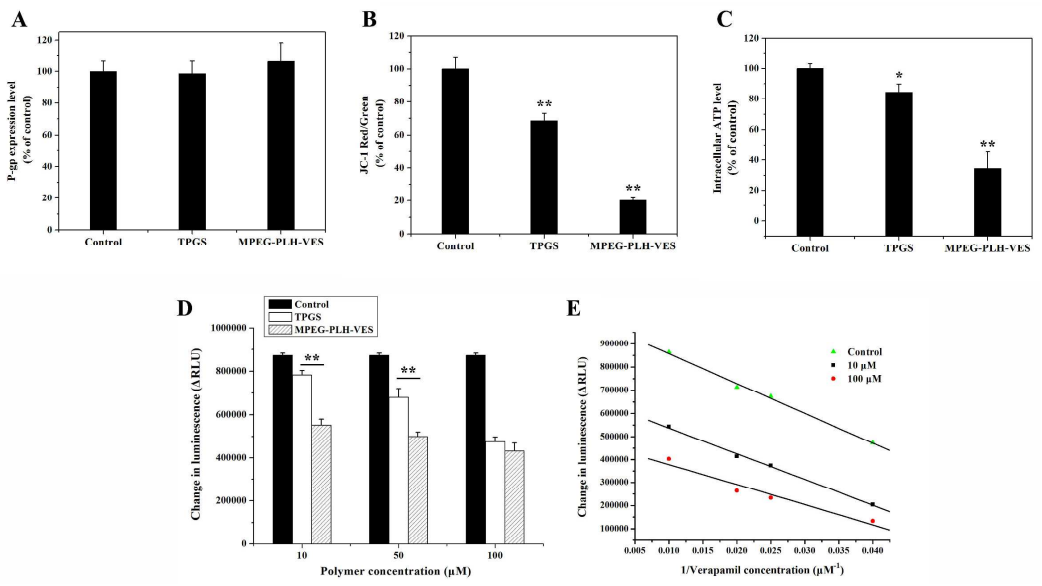


Figure 4 The effects of MPEG-PLH-VES or TPGS on the P-gp expression (A), mitochondrial membrane potential (B) and intracellular ATP level (C) of MCF-7/ADR cells. Inhibitory effect of MPEG-PLH-VES or TPGS on verapamil-stimulated P-gp ATPase activity (D) and the uncompetitive inhibitory mechanism of P-gp ATPase by MPEG-PLH-VES (E). * indicates $p < 0.05$; ** indicates $p < 0.01$.

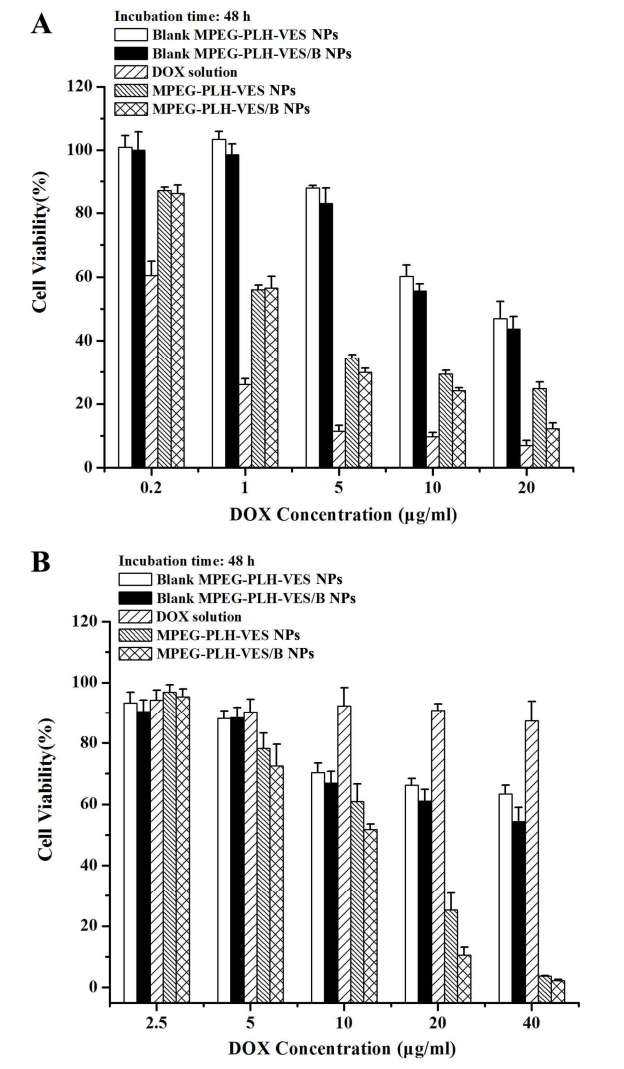


Figure 5 *In vitro* cytotoxicity of free DOX solution, DOX-loaded NPs and corresponding blank NPs against MCF-7 (A) and MCF-7/ADR (B) cancer cells after treatment for 48 h.

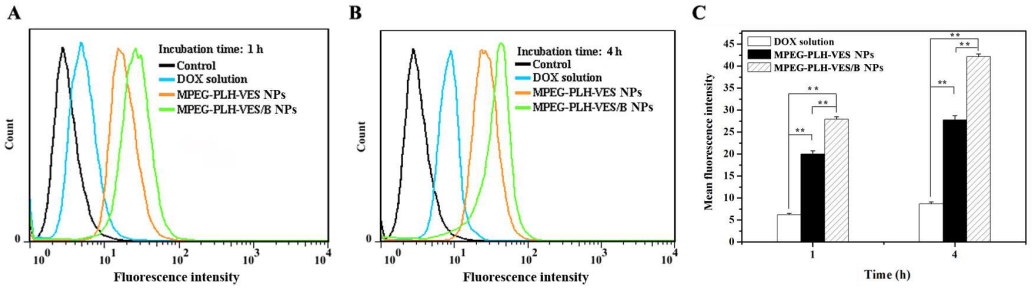


Figure 6 Flow cytometric histogram profiles of the intracellular uptake of DOX-loaded NPs and free DOX at 1 (A) and 4 h (B) in MCF-7/ADR cells and the fluorescence intensities of DOX accumulation after 1 and 4 h incubation (C). ** indicates $p < 0.01$.

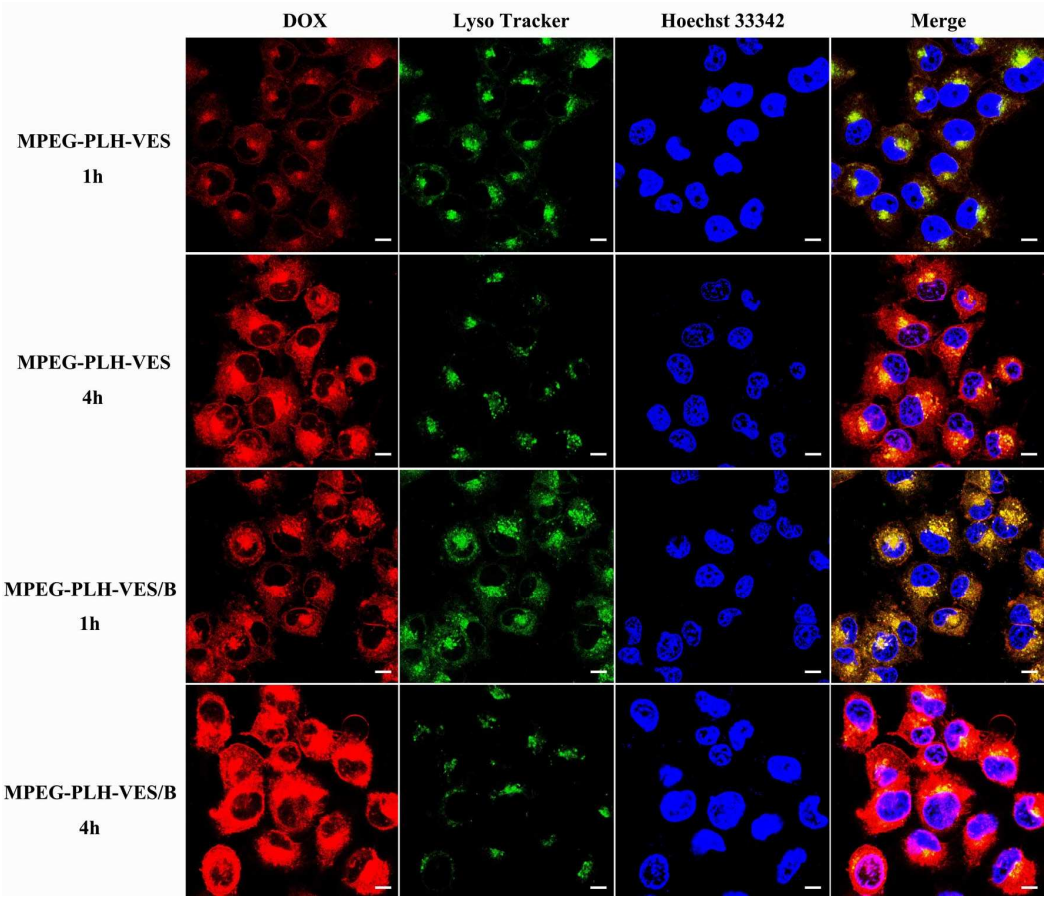


Figure 7 CLSM images of DOX-loaded MPEG-PLH-VES NPs and MPEG-PLH-VES/B NPs in MCF-7/ADR cells after 1 and 4 h incubation. For each panel, images from left to right show DOX (red), lysosomes stained by Lysotracker (green), cell nuclei stained by Hoechst 33342 (blue) and overlay of all images. (Scale bar: 10 μm)

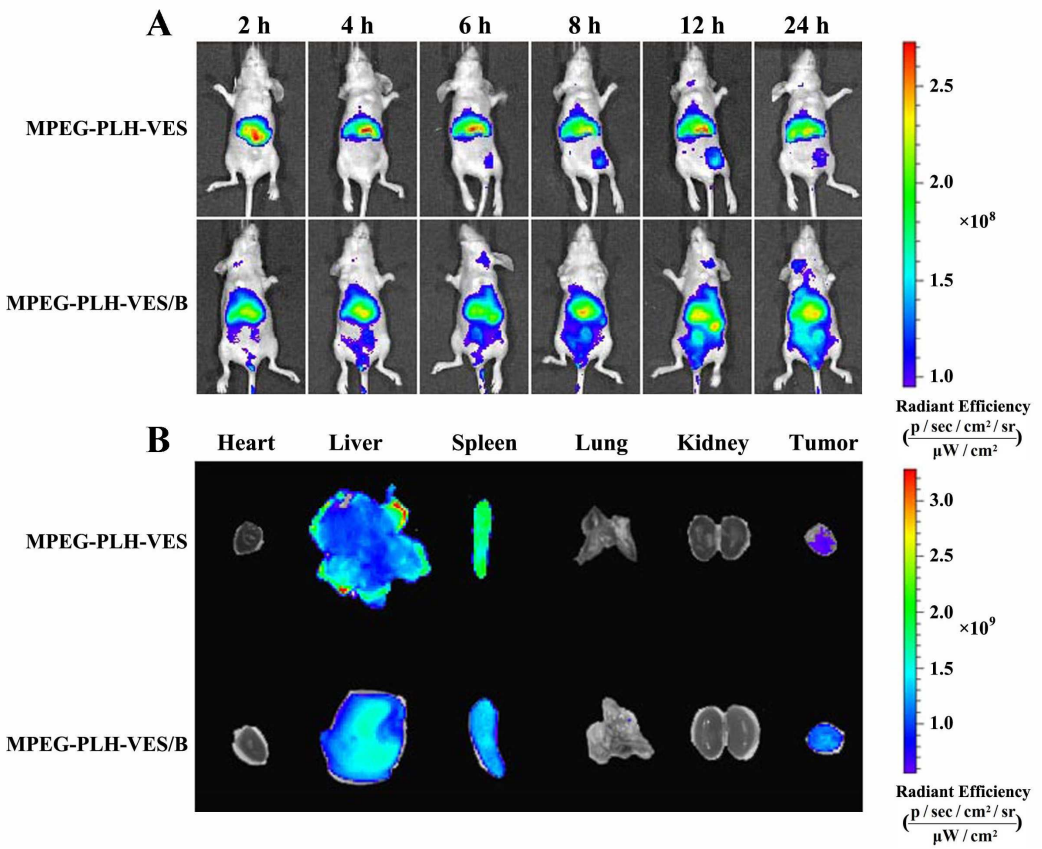


Figure 8 (A) *In vivo* imaging of MCF-7/ADR tumor-bearing nude mice injected with DiR-loaded MPEG-PLH-VES NPs and MPEG-PLH-VES/B NPs at 2, 4, 6, 8, 12 and 24 h post-injection, respectively. (B) *Ex vivo* imaging of DiR-loaded NPs in heart, liver, spleen, lung, kidney, and tumor of the nude mice bearing MCF-7/ADR tumor at 24 h post-injection, respectively.

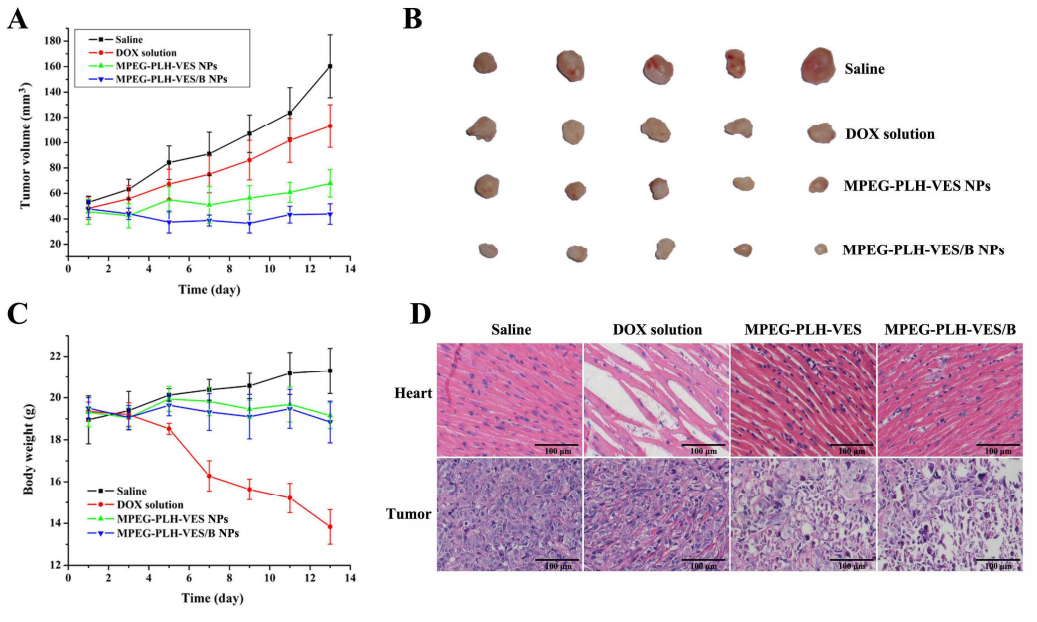


Figure 9 (A) Changes of tumor volume after treatment with saline, free DOX solution, DOX-loaded MPEG-PLH-VES NPs and DOX-loaded MPEG-PLH-VES/B NPs in MCF-7/ADR tumor-bearing nude mice. (B) The photos of excised tumor tissue from MCF-7/ADR tumor-bearing nude mice at the time of sacrifice. (C) Body weight changes of MCF-7/ADR tumor-bearing nude mice after intravenous injection of saline, DOX solution and DOX-loaded NPs. (D) Images of H&E-stained heart and tumor sections harvested from the mice after treatment with saline, free DOX solution and DOX-loaded NPs.

Table of Content/Abstract Graphic